IEEE Access
Multidisciplinary ⋮ Rapid Review ⋮ Open Access Journal

Received 17 October 2023, accepted 26 December 2023, date of publication 18 January 2024, date of current version 23 February 2024.

Digital Object Identifier 10.1109/ACCESS.2024.3355437

RESEARCH ARTICLE

Slope-Steering Motion Planning for Unmanned Tracked Vehicles Based on SSTP-RRT

YU ZHANG[1], XIXIA LIU[1], HONGQIAN CHEN[1], MIANHAO QIU[1], YUE ZHAO[1], AND XUDONG ZHANG[2], (Member, IEEE)

[1]Army Academy of Armored Force, Fengtai, Beijing 100072, China
[2]Beijing Institute of Technology, Haidian, Beijing 100051, China

Corresponding author: Xixia Liu (lxxljh@sina.com)

This work was supported in part by the National Natural Science Foundation of China under Grant 2020YFF0304000.

ABSTRACT Motion planning algorithms for unmanned tracked vehicles (UTV) which travel on off-road terrain often suffer from low accuracy and poor robustness when confronted with track sliding factor. SSTP-RRT (Slope-Steering Trajectory Parameter-space Rapidly-exploring Random Tree) motion planning algorithm is proposed for the slope-steering motion planning of UTV while considering the track sliding factor. A modified tracked vehicle slope-steering mechanical model is established to describe the process of UTV steering on the slope. The proposed UTV slope-steering model considers combined horizontal and vertical track sliding as well as steering centrifugal force. The PSO-LM (Particle Swarm Optimization - Levenberg Marquardt) algorithm is proposed to solve how to choose the initial values for the solution of the nonlinear system of equations of the model. The vehicle velocity, steering radii, and heading angle are taken as the independent variables, and the output rotational velocities of the inner and outer sprockets are taken as the dependent variables. The data are generated in a pre-computed way, and the output can be acquired by the point cloud surface fitting method based on moving least squares. By this method, UTV can travel according to the planned trajectory on the slope precisely and duly.

INDEX TERMS Unmanned tracked vehicle, slope steering, motion planning, SSTP-RRT.

I. INTRODUCTION

The tracked vehicle is the vehicle of choice for an autonomous task requiring off-road mobility [1]. There is an urgent demand for UTV with a large load capacity in the off-road environment [2], [3]. A reliable and efficient motion planning algorithm is the core of unmanned vehicle navigation technology, and a key technology reflecting their level of intelligence [4]. Compared to structured environments, the unmanned vehicle must consider more constraints for motion planning in complex off-road unstructured environments, such as terrain conditions and dense obstacles. Most tracked vehicles are skid-steering, and the sliding caused by changes in velocity at various points on the track as well as the compression and shear of the terrain would be key factors in determining the steering of UTV, with a large impact on accurate motion planning.

Owing to the effect of slope resistance, slope-steering can make tracked vehicles produce greater sliding than steering on flat terrain. Motion planning for UTV slope-steering must take full account of the effect of tracks sliding on the planned trajectory. If an UTV is planning according to flat terrain when slope-steering, the trajectory may deviate significantly from the plan, resulting in collisions with obstacles, failure to pass smoothly according to the planned trajectory, or even instability and loss of control.

Based on the mechanism of track-terrain interaction, an accurate UTV slope-steering model can generate the control outputs of both sprockets according to the path and velocity values generated from trajectory planning. It will help UTV to complete accurate motion planning when slope-steering, while considering the sliding factor, which also facilitates the trajectory tracking control of the

The associate editor coordinating the review of this manuscript and approving it for publication was Ludovico Minati.

UTV, taking into account vehicle characteristics and terrain properties.

We summarize relevant research on the path, trajectory, and motion planning for UTV, which provides theoretical and methodological references. Zhu et al. established a kinematic model to overcome vertical obstacles based on a multi-sectional tracked mining search robot, and proposed an inverse kinematic optimization algorithm for a robot overcoming obstacles based on a three-level, four-group nested artificial fish swarm algorithm [5]. Ping et al. designed a DSP (Digital Signal Processing)-based search tracked mobile robot, modeled the environment with the help of the path map method, and solved the redundancy problem of motion point sequence selection based on the improved RRT algorithm with good planning results [6]. Jia et al. studied a real-time path planning algorithm combining rolling window theory and an ant colony algorithm for a tracked robot with known location environment information [7]. Gao et al. established an environment model based on Voronoi diagrams for a tracked robot and used a heuristic search algorithm similar to the A* algorithm (see below) to solve for the extreme values of the evaluation function to plan the optimal path, with the highest safety and efficiency as the search criteria [8]. Wang et al. proposed a motion planning method that generates motion primitives offline based on the kinematic characteristics of different configurations and selects primitives online to generate trajectories that well match vehicle motion patterns for the unified motion planning problem of heterogeneous UTV [9]. Zhou et al. introduced the A* algorithm for optimal path planning of an UTV under a global map, with the shortest path as the search principle, and used a cubic B spline to smooth the obtained paths [10]. Deng et al. developed an improved A* algorithm with heading constraints based on a tracked demolition robot platform, which eliminated the heading jitter problem and was combined with B-sample smoothing of paths to achieve optimal path planning [11]. Sun et al. proposed a dynamic window method with heuristic function alteration [12]. Aiming at the characteristics of large UTV and the difficulty of turning, a curvature heuristic function reduced the number of turns, and a combined path planning method based on an improved ant colony algorithm and dynamic window method was proposed.

There has been less research on motion planning for UTV. Most have focused on path and trajectory planning, a few motion planning studies have considered kinematic constraints, and fewer have considered dynamics constraints. No research has been conducted on UTV slope-steering motion planning considering sliding factors. To achieve accurate motion planning for UTV slope-steering, an accurate model must be established [14].

II. UTV SLOPE-STEERING MODIFIED MODEL CONSIDERING SLIDING AND CENTRIFUGAL FORCE

The accuracy of the model is reflected in the prediction of the amount of track sliding. The proposed UTV slope-steering model considers combined horizontal and vertical track sliding as well as steering centrifugal force.

We make the following assumptions [15]:

(1) The tracked vehicle is in steady-state uniform steering motion on a tight slope terrain, and the shear force between the track and terrain is related to the shear displacement at that point in the steering process, in the direction opposite to that of the sliding velocity of the track at that point;

(2) The coefficient of resistance is the same as when traveling in a straight line;

(3) The component of the shear force between the track and terrain in the longitudinal direction constitutes the traction and braking force of the tracks, the component in the transverse direction constitutes the transverse resistance, and the moment of the transverse resistance on the steering center constitutes the steering resisting moment.

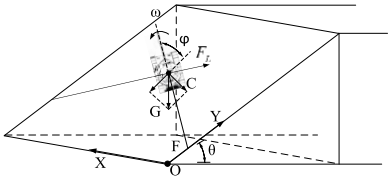

FIGURE 1. Schematic diagram of overall force when a UTV is slope-steering.

Figure 1 shows the overall force diagram of UTV slope-steering with a heading angle of φ. Using the sloping plane as the basic plane and establishing the XOY geodesic coordinate system as shown, φ is the angle between the vehicle's longitudinal symmetry axis and the Y-axis [16]. The specific force situation of the vehicle is shown in Figure 2.

The vehicle coordinate system is established using the body form center as the coordinate origin, and the equivalent longitudinal slope angle α and equivalent lateral slope angle β of the vehicle are defined by

$$\tan\alpha = \tan\theta\cos\varphi \tag{1}$$

$$\tan\beta = \tan\theta\sin\varphi \tag{2}$$

Vehicle gravity is divided between that perpendicular and parallel to the slope. The parallel slope splitting force is

$$G_Y = mg\sin\theta, \tag{3}$$

with vertical slope component

$$G_Z = mg\cos\theta \tag{4}$$

The steering centrifugal force has components

$$\mathrm{F}_{LX'} = \frac{mv^2}{R}\sin\varphi \tag{5}$$

$$\mathrm{F}_{LY'} = \frac{mv^2}{R}\cos\varphi \tag{6}$$

According to Figure 2, the forces in each pair of points take moments to C_2.

$$F_{LX'} \times h_g + G_z \times (\frac{B}{2} + c_x) = N_2 \times B$$

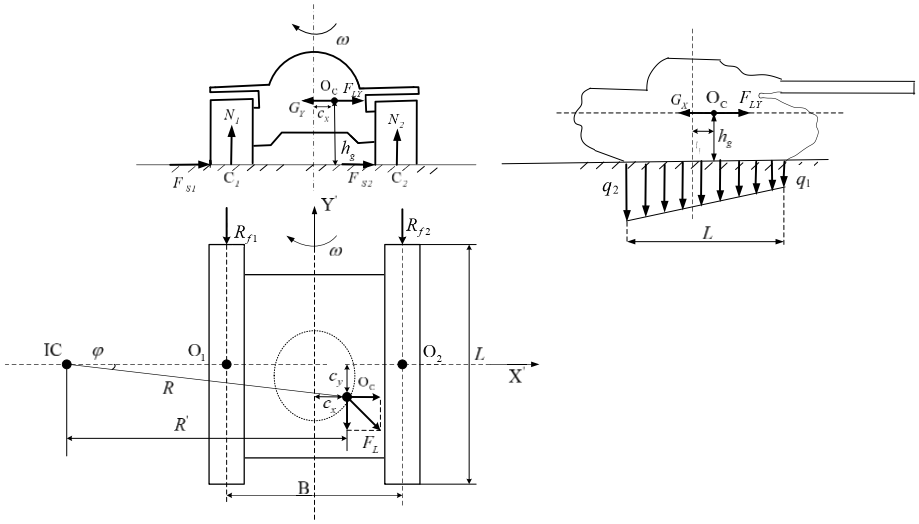

FIGURE 2. Forces on a slope-steering UTV when centrifugal force is taken into account.

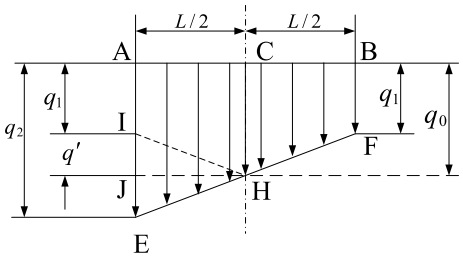

FIGURE 3. Schematic diagram of load distribution on track.

The outer track load is found to be

$$N_2 = \frac{mv^2h}{RB} \times \cos\varphi + mg\sin\theta \times (\frac{1}{2} + \frac{c_x}{B}) \tag{7}$$

Similarly taking the moments for point C_1, the inner track load is

$$N_1 = mg\sin\theta \times (\frac{1}{2} - \frac{c_x}{B}) - \frac{mv^2h}{RB} \times \cos\varphi \tag{8}$$

According to Figure 2, the load distribution on the track can be obtained as shown in Figure 3.

The forces of quadrilaterals ACHI and CBFH cancel each other by taking moments at point C in the center of the track, so it is sufficient to calculate the moment taken by the forces of the triangle IHE at point C, whose area is

$$\Delta\text{IHE} = \frac{1}{2}(\text{q}_2\text{-q}_1) \times \frac{L}{2} \tag{9}$$

From the moment balance, we find

$$F_{LY'} \times h_g + G_Z \times c_y = \Delta IHE \times \frac{2}{3} \times \frac{L}{2} \tag{10}$$

So,

$$q_2 - q_1 = \frac{12}{bL^2}\left(F_{LY'} \times h_g + G_Z \times c_y\right) \tag{11}$$

According to equation (7), it can be obtained that

$$q_2 + q_1 = \frac{2N_1}{bL}, \tag{12}$$

and combining equations (11) and (12) yields

$$\begin{cases} q_2 = \dfrac{N_1}{bL} + \dfrac{6}{bL^2}(F_{LY'} \times h + G_Z \times c_y) \\ q_1 = \dfrac{N_1}{bL} - \dfrac{6}{bL^2}(F_{LY'} \times h + G_Z \times c_y) \end{cases} \tag{13}$$

For any point y_1 on the track, the terrain pressure is

$$q_{y_1} = \frac{N_1}{bL} - \frac{12}{bL^3}(F_{LY'} \times h + G_Z \times c_y)(y_1 + D - c_y) \tag{14}$$

Similarly, the terrain pressure at any point y_2 on the outer track can be found as

$$q_{y_2} = \frac{N_2}{bL} - \frac{12}{bL^3}(F_{LY'} \times h + G_Z \times c_y)(y_2 + D - c_y) \tag{15}$$

When the vehicle is moving around the instantaneous center of steering with angular velocity $\dot{\varphi}$, the drafting velocities at corresponding points, O_1 and O_2 on the centerline of the tracks on both sides are

$$v_{oiyi} = (R' \mp \frac{B}{2} + c_x)\dot{\varphi} \quad i = 1, 2 \tag{16}$$

Any point (x_i, y_i) on the longitudinal centerline of the track corresponds to a steering motion with an angular velocity around the point, O_1 and O_2, so that the relative velocity component of the point in the transverse direction is $y\dot{\varphi}$. In a fixed coordinate system, the velocity component of the sliding velocity of point (x_i, y_i) in the transverse direction can be expressed as

$$q_{y_1} = \frac{N_1}{bL} - \frac{12}{bL^3}(F_{LY'} \times h + G_Z \times c_y)(y_1 + D - c_y) \tag{17}$$

Similarly, the velocity component in the longitudinal direction can be found as

$$q_{y_2} = \frac{N_2}{bL} - \frac{12}{bL^3}(F_{LY'} \times h + G_Z \times c_y)(y_2 + D - c_y) \quad (18)$$

The time taken to drive off the terrain at any point on the track is

$$v_{oiyi} = (R' \mp \frac{B}{2} + c_x)\dot{\varphi} \quad i = 1, 2 \quad (19)$$

Therefore, the shear displacement between the track and terrain in the coordinate system X′OY′ at any point (x_i, y_i) on both tracks can be calculated as the component in the X′ direction,

$$\begin{aligned} j_{X'i} &= \int_0^t v_{jX'i}dt = \int_y^{L/2} \{-\left[\left(R' \mp B/2 + c_x\right)\dot{\varphi} - r_z\omega_i\right]\dot{\varphi} \\ &\quad \sin\varphi - y_i\dot{\varphi}\cos\varphi\} \frac{\mathrm{d}y}{r_z\omega_i} \\ &= \left(R' \mp B/2 + c_x\right)(\cos\varphi - 1) - y_i\sin\varphi \; i = 1, 2 \end{aligned} \quad (20)$$

Similarly, the shear displacement in the Y′ direction is

$$\begin{aligned} j_{Y'i} &= \int_0^t v_{jY'i}dt = \int_y^{L/2} \{-\left[\left(R' \mp B/2 + c_x\right)\dot{\varphi} - r_z\omega_i\right] \\ &\quad \cos\varphi - y_i\dot{\varphi}\sin\varphi\} \frac{\mathrm{d}y}{r_z\omega_i} \\ &= \left(R' \mp B/2 + c_x\right)\sin\varphi - L/2 + y_i\cos\varphi \quad i = 1, 2 \end{aligned} \quad (21)$$

The total shear displacement can be expressed as

$$j_i = \sqrt{j_{Xi}^2 + j_{Yi}^2} \quad i = 1, 2 \quad (22)$$

When a UTV travels, the shear force between the track and terrain is related to the amount of relative sliding between them, and the shear stress between the track and terrain can be calculated using equations (6) - (9). The sheer force between the track and the terrain is in the opposite direction to the sliding velocity of the track, as shown in Figure 4.

The shear force per unit area of the track can be calculated as

$$dF_i = \tau_i dA = p_i\mu\left[1 - \exp(-j_i/K)\right]dA \quad i = 1, 2, \quad (23)$$

the longitudinal force of the shear action between the track and terrain can be found as

$$\begin{aligned} F_{yi} &= \int dF_i \sin(\pi + \delta_i) \\ &= -b\int_{-L/2}^{L/2} p_i(y_i)\mu\left[1 - \exp\left(-j_i/K\right)\right]\sin\delta_i dy \;\; i = 1, 2 \end{aligned} \quad (24)$$

where, δ_i is the angle between the sliding velocity and the direction of the X′-axis at any point on the high- and low-velocity tracks.

The lateral forces acting on both tracks are

$$\begin{aligned} F_{xi} &= \int dF_i \cos(\pi + \delta_i) \\ &= -b\int_{-L/2}^{L/2} p_i(y_i)\mu\left[1 - \exp\left(-j_i/K\right)\right]\cos\delta_i dy \;\; i = 1, 2 \end{aligned} \quad (25)$$

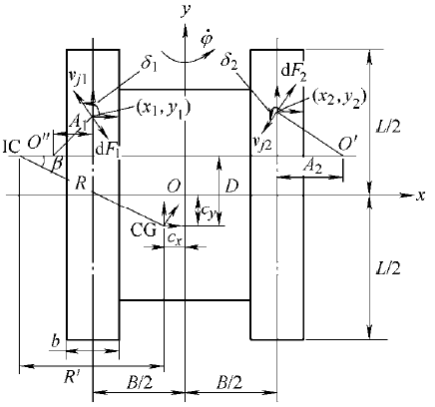

FIGURE 4. Kinematic relationship between tracks on both sides during steady-state steering.

The steering drive moment can be calculated by taking the moment of the longitudinal force of both tracks at the point O_v. The steering resistance moment can be calculated by taking the moments of the lateral forces of the tracks on each side at points O_1, O_2 where the tracks meet, i.e., the intersection of the longitudinal centerline of the vehicle and the transverse line across its steering center, as shown in Figure 5.

The steering drive torque on both tracks is

$$\begin{aligned} M_{D_i} &= \int dF_i \sin(\pi + \delta_i)B \\ &= -\frac{1}{2}b\int_{-L/2}^{L/2} Bp_i(y_i)\mu\left[1 - \exp(-j_i/K)\right]\sin\delta_i dy \;\; i = 1, 2, \end{aligned} \quad (26)$$

and the steering resistance moments on both tracks is

$$\begin{aligned} M_{\mu_i} &= \int dF_i \cos(\pi + \delta_i)y_i \\ &= -\frac{1}{2}b\int_{-L/2}^{L/2} y_i p_i(y_i)\mu\left[1 - \exp(-j_i/K)\right]\cos\delta_i dy \;\; i = 1, 2 \end{aligned} \quad (27)$$

The slip angle of the track sliding velocity in equations (26) and (27) is determined from the kinematic relationship in Figure 4 [15],

$$\begin{aligned} \sin\delta_i &= \frac{v_{jyi}}{\sqrt{v_{jxi}^2 + v_{jyi}^2}} \\ &= \frac{\left(R' \mp B/2 + c_x\right)\dot{\varphi} - r_z\omega_i}{\sqrt{\left[\left(R' \mp B/2 + c_x\right)\dot{\varphi} - r_z\omega_i\right]^2 + (y_i\dot{\varphi})^2}} \quad i = 1, 2 \end{aligned} \quad (28)$$

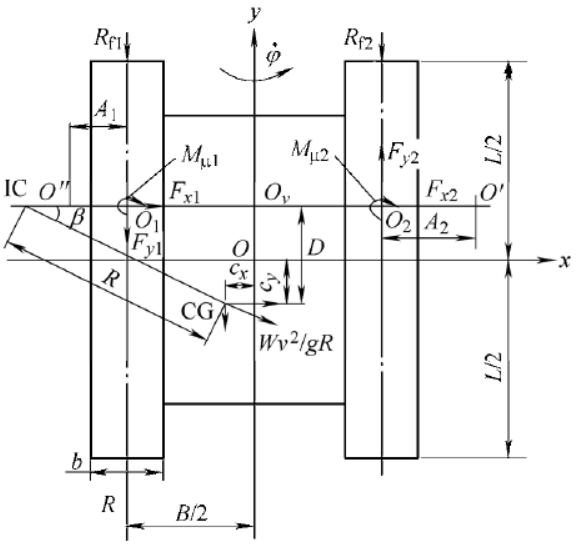

FIGURE 5. Schematic diagram of resistance moments and forces acting on both tracks when slope-steering.

$$\cos\delta_i = \frac{v_{jxi}}{\sqrt{v_{jxi}^2 + v_{jyi}^2}} = -\frac{-y_i\dot{\varphi}}{\sqrt{\left[\left(R' \mp B/2 + c_x\right)\dot{\varphi} - r_z\omega_i\right]^2 + (y_i\dot{\varphi})^2}} \quad i = 1, 2 \tag{29}$$

where, v_{jyj} and v_{jxj} are respectively the longitudinal and lateral sliding velocity of both tracks in the vehicle coordinate system.

In the steady-state steering process of the UTV, the force on the track and the vehicle force are in equilibrium. According to the force balancing relationship between the tracking force and torque in the axial directions X′ and Y′ of the reference coordinate system, as well as the moment balancing the relationship between the force and point O_v, we can use eq. (24)–(27) to obtain the slope steering equations of motion,

$$\sum F_x = 0F_{x_2} + F_{x_1} - \frac{mv^2}{gR}\cos\beta + \mathrm{mgsin}\theta\sin\varphi = 0 \tag{30}$$

$$\sum F_y = 0F_{y2} + F_{y1} - \frac{mv^2}{gR}\sin\beta - \left(R_{f1} + R_{f2}\right) - mg\sin\theta\cos\varphi = 0 \tag{31}$$

$$\sum M_{ov} = 0\, M_{D2} - M_{D1} - \frac{B}{2}\left(R_{f2} - R_{f1}\right) + \left(D\cos\beta + c_x\sin\beta\right)\frac{mv^2}{gR} - mg\sin\theta\left(D\sin\varphi - \cos\varphi c_x\right) = M_{\mu_2} + M_{\mu_1} \tag{32}$$

where, R_{f1} and R_{f2} are the resistance to movement of both tracks, and f_r is related to the normal load of the tracks on both sides and the road resistance factor by

$$R_{fi} = m\left[\frac{1}{2} \mp \left(\frac{h}{B}\frac{v^2}{gR}\cos\beta - \frac{c_x}{B}\right)\right]f_r \quad i = 1, 2 \tag{33}$$

Given the structural parameters of the vehicle, track center B, track width b, track terrain length L, vehicle mass m; terrain condition parameters, μ, K, c, φ, slope angle θ; vehicle driving condition parameters, desired vehicle velocity v, desired steering radii R, and vehicle heading angle φ; track slip rate; and skid rate; the sprocket output during UTV slope-steering can be calculated.

III. PSO-LM ALGORITHM TO SOLVE UTV SLOPE-STEERING MODEL

As UTV slope-steering model is a complex transcendental equation, analytical solutions cannot be found exactly, and can only be solved using numerical iterations. When solving a nonlinear system of equations, conventional algorithms such as Newton's method, the Gauss-Newton method, and the LM algorithm all rely heavily on the selection of initial values, which can produce solutions that vary considerably. We use a combined PSO and LM algorithm, PSO-LM.

The algorithm starts by finding an approximation to the model solution via a PSO algorithm, which is used as an initial value in the LM algorithm for the exact solution of the model. The feasible interval of the solution is set according to the constraints of the model, and the starting point is generated by a global search and a multi-start method, using a local solver to find the optimal solution.

PSO can continuously plan new location points by continuously and iteratively learning historical best values to eventually find the best location values [16]. However, owing to random uncertainty in the particles, although their global search capability is greatly improved, it can make their local search capability poor. Therefore, a strong global search capability is needed at the beginning of the algorithm, and the whole particle population should have a strong local search capability at the end. Therefore, PSO-LM uses PSO to calculate the initial value range before applying LM to find the numerical solution for nonlinear minimization. LM is an optimization method for least-squares estimation of regression parameters in nonlinear regression that provides a numerical solution for nonlinear minimization and can improve the problem of nonexistent inverse matrices of the Gauss-Newton algorithm [17], [18]. LM combines the Gauss-Newton algorithm and the gradient descent method by modifying the parameters during iteration, ensuring a velocity of convergence while searching along the descent direction overall.

The flow of the PSO-LM algorithm for the UTV slope-steering model solution is shown in Figure 6.

IV. INTEGRATED SLIDING ANALYSIS OF UTV SLOPE-STEERING

A. INTEGRATED SLIDING ANALYSIS FOR UTV SLOPE-STEERING AT DIFFERENT SLOPE ANGLES

After considering the combined sliding and steering centrifugal forces, a quantitative analysis was conducted for the slope angle and the amount of slope steering deviation of the UTV. In a steering condition with vehicle velocity $v = 2$ m/s and steering radii $R = 20$ m, plane and slope angles $\theta = 3°$, 5°, 8°, 10°, and 12° were selected for comparative simulation analysis. Figure 7 shows the results of the comparison between the sprockets' output velocity and the actual velocity conversion (sprocket velocity) of the vehicle.

In Figures 7 and 8, the red dashed line indicates the driving velocity, and the solid lines with symbols indicate the output velocity at different slope angles. It can be seen that during UTV slope-steering, the actual velocity of the outer track is less than the output velocity, resulting in slipping, and the actual velocity of the inner track is greater than the output velocity, resulting in skidding. The outer track slip rate difference is mainly in the third and fourth quadrants, and the inner track skid rate difference is mainly in the first and second quadrants.

To quantify and analyze the deviation of output velocity from driving velocity, and to develop trajectory optimization criteria, we evaluate using the root mean square error (RMSE),

$$RMSE = \sqrt{\frac{\sum_{i=1}^{n} (p_i - a_i)^2}{n}} \tag{34}$$

where p_i is the predicted target value, which here is the actual driving conversion velocity of the vehicle; a_i is the actual target value, which refers to the output velocity of the driving wheels; and n is the number of samples.

The RMSE values for each location point are shown in Table 1.

To visualize the difference between the output velocity and driving velocity, the output velocity on both sprockets is converted to the theoretical steering radii of the UTV, which is compared to the desired steering radii of $R = 20$ m, as shown in Figure 9. Figure 10 shows the theoretical steering radii in polar coordinates.

As shown in Figures 9 and 10, the calculated theoretical steering radii are calculated to be less than the desired steering radii because the inner track skids and the outer track slips. However, unlike flat steering, where the steering radii remain stable, the variation varies considerably during slope steering, where the radii change with the heading angle (HA).

The maximum/minimum values of the steering radii (max R/min R) at different slope angles and the corresponding heading angles are shown in Table 2.

As shown in Table 2, the UTV is more prone to instability when traveling in the third quadrant. When the UTV is steering upwards on a downhill slope, the region should be focused when developing an UTV trajectory optimization strategy. In summary, as the slope angle increases, the deviation between the theoretical and desired steering radii increases, indicating more track sliding. To follow a prescribed steering radius, an UTV must use control commands that differ significantly from the plan.

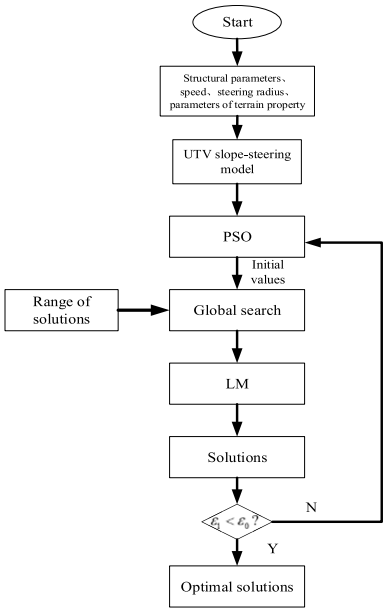

FIGURE 6. Flowchart for solving UTV slope-steering model based on PSO-LM algorithm.

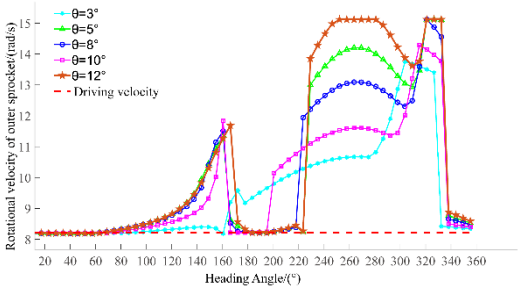

FIGURE 7. Output velocity of outer sprocket versus driving velocity at different slope angles.

B. INTEGRATED SLIDING ANALYSIS OF UTV SLOPE-STEERING AT DIFFERENT VELOCITIES

The slope steering model established in this paper takes into account the steering centrifugal force, which increases with vehicle velocity. We analyze the amount of deviation of the steering radii of UTV slope steering at different driving velocities. With a steering radii of R=20 m and a slope angle of $\theta = 5°$, vehicle velocities of $v = 2$ m/s, 4 m/s, 6 m/s, and 8 m/s were selected for simulation, with results as shown in Figures 11 and 12.

It can be seen that during slope steering, the outer track slips and the inner track skids. The amount of track slippage increases the vehicle velocity, indicating that the greater

TABLE 1. Output velocity of inner and outer sprockets at different slope angles versus driving velocity RMSE.

	θ=3°	θ=5°	θ=8°	θ=10°	θ=12°
Inner sprocket	1.3902	2.5002	2.2579	1.7108	2.5995
Outer sprocket	2.0775	3.2140	2.8518	2.3864	3.6483

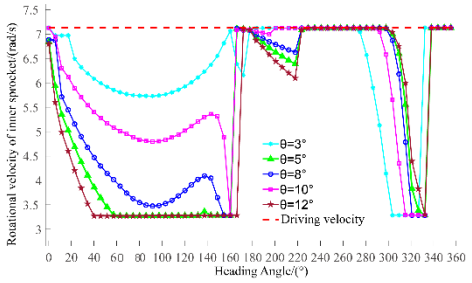

FIGURE 8. Output velocity of inner sprocket versus driving velocity at different slope angles.

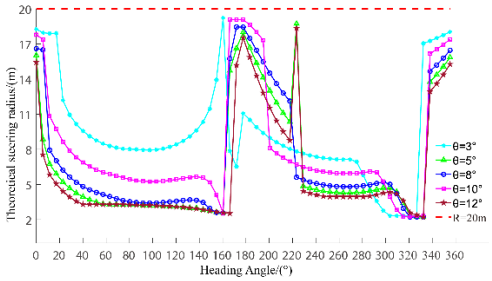

FIGURE 9. Comparison of steering radii at different gradient slope angles.

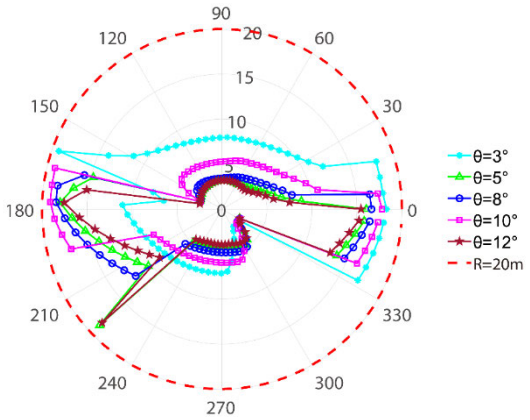

FIGURE 10. Comparative polar plot of steering radii at different slope angles.

the velocity the greater the tracking force required on both sides of the UTV when slope-steering. For the outer track, the overlap between output velocity and driving velocity is higher in the first and second quadrants and decreases with increasing velocity. For the inner track, the overlap between output velocity and driving velocity is higher in the third and fourth quadrants and increases with velocity. The trend in the theoretical steering radii for output velocity conversion is shown in Figures 13 and 14. Based on the analysis of the RMSE index, follows as Table 3.

As shown in Figures 13 and 14, the steering radii increases with the vehicle velocity. When $v = 4$ m/s, the steering radii and desired radii in the interval of 20°–120° largely coincide. This indicates that in the region where slope resistance and steering centrifugal force act in opposite directions, they can partially or fully cancel out, helping the vehicle to better follow the planned steering radii. At the same time, in areas where the slope resistance and steering centrifugal force act in the same way, the steering centrifugal force will be superimposed on the vehicle with the slope resistance, requiring a greater velocity difference to produce shear forces and greater deviation in the UTV trajectory. Therefore, when an UTV is slope-steering, the first and second quadrants should be chosen for steering as far as possible, and choosing the right driving velocity will improve the vehicle's performance in driving according to the planned steering radii. When steering in the third and fourth quadrants, the vehicle velocity should be reduced as much as possible to limit the adverse effects of steering centrifugal force.

According to the above analysis, the theoretical and actual steering radii of an UTV on a slope differ significantly. If the slope factor is not taken into account during trajectory planning, the planned trajectory will deviate significantly from the actual driving trajectory, and correcting the deviation through sensors and controllers will consume computing power, time, and driving velocity, which will have an impact on the mobility of the UTV, so it is necessary to incorporate the UTV slope-steering model in trajectory planning, for which we choose the TP-RRT algorithm to efficiently detect collision-free, kinematically-feasible paths for vehicles of arbitrary shape, which can enable the UTV to smoothly pass through obstacle-laden off-road areas [19], [20].

To meet the slope driving requirements of the UTV, the driving velocity, steering radii, and heading angle are brought into equations (30)–(32) to find the values of the sprocket output velocity on both sides at a specific slope angle, so that the UTV can drive according to the planned trajectory. As solving this set of equations takes some time, it cannot meet the real-time driving requirements of the UTV. Therefore, we adopt pre-calculation, taking the three variables of vehicle velocity, steering radii, and heading angle as input, and the

TABLE 2. Maximum/minimum steering radii at different slope angles and corresponding heading angles.

SLOPE ANGLE	MAX R (M)	HA (°)	MIN R (M)	HA (°)
θ=3°	19.2255	160.4282	2.3115	303.6676
θ=5°	18.7265	233.4535	2.2090	332.3155
θ=8°	18.4478	171.8873	2.2087	320.8654
θ=10°	19.0897	166.1578	2.2676	315.1268
θ=12°	18.3402	223.4535	2.2125	332.3155

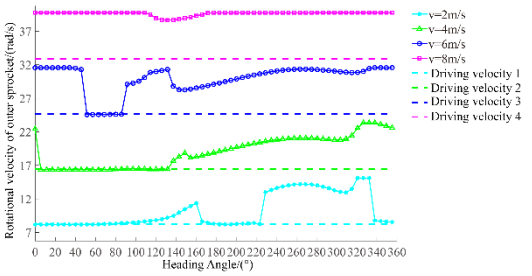

FIGURE 11. Output velocity of outer sprocket versus driving velocity at different velocities.

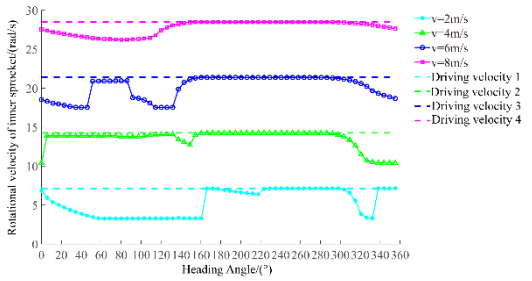

FIGURE 12. Output velocity of inner sprocket versus driving velocity at different velocities.

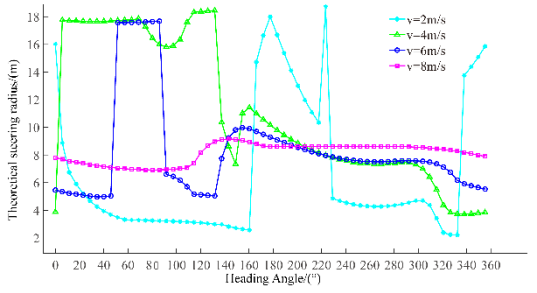

FIGURE 13. Theoretical slope-steering radii of UTV at different velocities.

sprocket rotational velocity on both sides as output, constructing a three-dimensional look-up table (LUT) and realizing the rotational velocity output in real-time based on the point cloud surface fitting algorithm of the moving least-squares method to improve the timeliness of the motion planning algorithm.

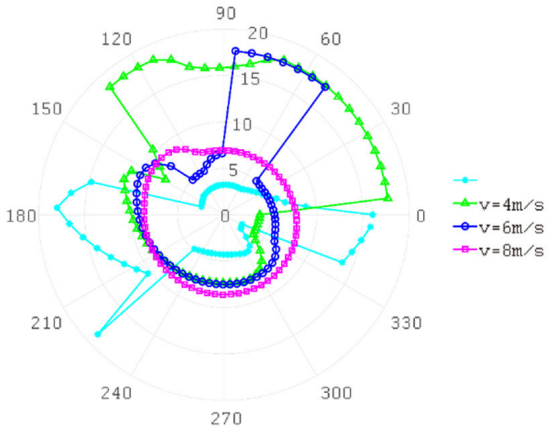

FIGURE 14. Theoretical slope-steering radii of UTV at different velocities in polar coordinates.

The method is to obtain an approximation of the target point using a fitting algorithm. In the preparation of the LUT, the calculation steps for vehicle velocity, steering radii, and heading angle do not need to be the same because the three independent variables do not have the same influence on the dependent variable. For independent variables that have a small effect on the dependent variable, the step size can be enlarged, and for those that have a large effect, the step size can be shortened to ensure the accuracy of the fitting algorithm while reducing the amount of data required.

To quantify the influence of the independent variables on the dependent variable of the UTV slope-steering model, a global sensitivity analysis is used to rank the sensitivity of the independent variables to the dependent variable and design reasonable calculation steps for the independent variables.

In summary, for the UTV slope-steering model, the three variables, the vehicle velocity is the most sensitive, with a PAWN index value more than twice those of the steering radii and heading angle, while the vehicle velocity and heading angle are about equally sensitive [21], [22]. Therefore, when preparing the LUT for UTV slope-steering motion planning, divisions of 0.5 were used for the vehicle velocity, and 1 for the steering radii and heading angle. The data table is prepared as shown in Figure 15.

TABLE 3. Actual and theoretical RMSE values for sprocket velocities on both sides at different velocities.

	v=2 m/s	v=4 m/s	v=6 m/s	v=8 m/s
Inner	2.5002	1.3777	1.9412	1.1491
Outer	3.214	3.5339	5.6563	6.7705

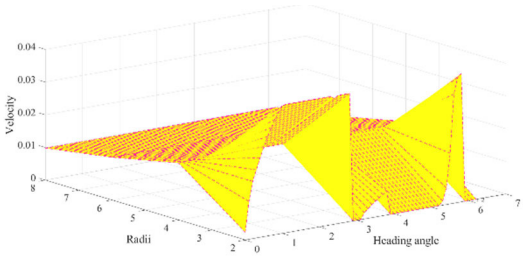

FIGURE 15. Prepared 3D LUT datasheet.

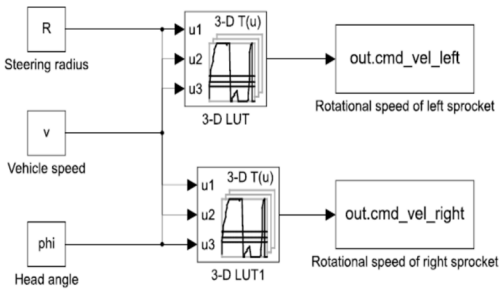

FIGURE 16. 3D LUT verification diagram based on Simulink.

The basic process is as follows. After the UTV has sensed the environment and established a global map, information such as obstacles, starting points, and slope angles are input to the trajectory planning algorithm to generate a collision-free trajectory containing information such as location points, vehicle linear and angular velocity, steering radii, and heading angle. The trajectory is then calculated as a 3-point pre-calculated value. The pre-calculated values are compiled into a 3D LUT, and the TP-RRT-generated trajectory is fitted with the 3D LUT difference to generate the left and right sprocket control velocities, ultimately realizing the motion planning of the UTV. Figure 16 shows the process validation of the Simulink-based implementation of the 3D LUT.

V. EXPERIMENT

Experiments were conducted on a self-developed UTV platform with laser SLAM mapping capability to achieve cm-level high-precision navigation mapping. The platform also fuses laser odometry, IMU, and RTK through EKF to make initial projections of the UTV's position and ultimately achieve its precise positioning. The platform is shown in Figure 17.

FIGURE 17. Experimental platform for UTV.

The slope of the asphalt road in front of the Vehicle Engineering Department of the Army Academy of Armored Forces (China, Beijing) was chosen as the experimental site, with a slope angle of 12.13°. The slope-steering model established in this paper is applicable to a solid paved road [21]. Before the start of the experiment, a 3D point cloud high-precision map of the site was established by laser SLAM, as shown in Figure 18(b).

A. EXPERIMENT ON FIXING THE VELOCITY OF BOTH SPROCKETS OF THE UTV

Before conducting the SSTP-RRT algorithm validation experiments, the slope-steering sliding effect of the UTV was verified. The UTV velocities of both sprockets were fixed at 0.5 m/s and 0.2567 m/s. The UTV traveled three laps. Figure 19 shows the linear velocity converted from both sprockets' velocities, with laps represented by different colors. There is a slight oscillation in velocity due to the motor output, but the overall velocity remains constant. Figure 20 shows a graph of the change in heading angle as the vehicle travels for three circles, with the heading angle changing periodically.

In Figure 21, the solid line represents the actual trajectory of the vehicle, the arrow represents the direction of travel, the asterisk represents the position of the center of the circle estimated according to the actual trajectory of the vehicle, and the dashed line represents the theoretical steering trajectory circle calculated according to the velocity of the UTV. As shown in the diagram, on a flat surface, the UTV will theoretically

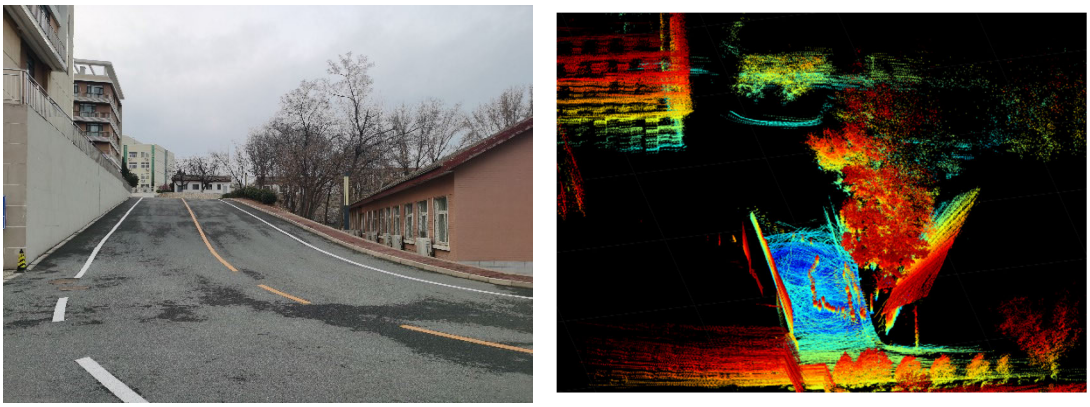

(a) Photos (b) High-precision 3D point cloud map

FIGURE 18. Comparison of real view of the experimental site with point cloud map.

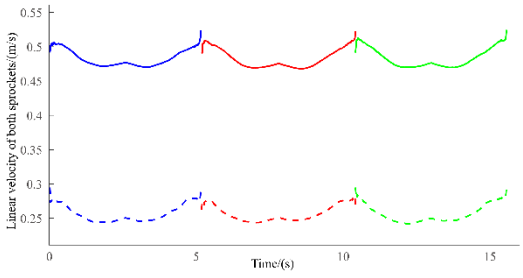

FIGURE 19. Measured variation of both sprockets' velocity.

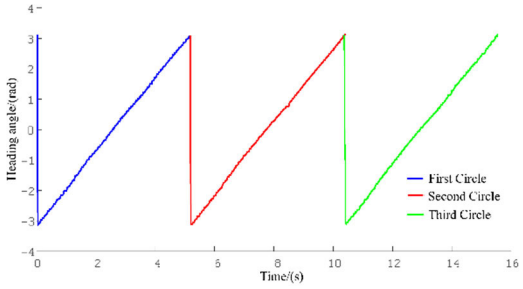

FIGURE 20. Traveling heading angle diagram of UTV.

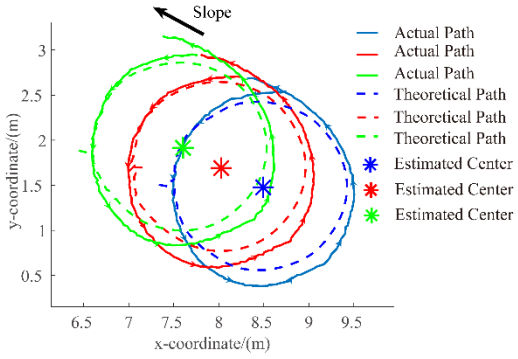

FIGURE 21. Trajectory after fixing the velocity of both sprockets.

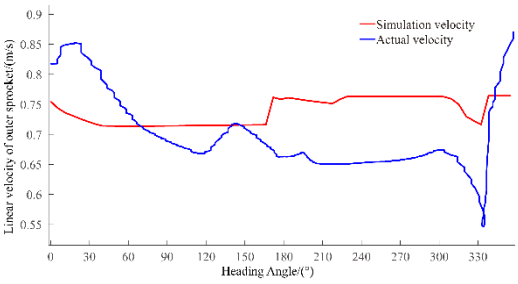

FIGURE 22. Comparison between commanded and actual outer sprocket linear velocity.

draw a complete circular trajectory when both sprockets are traveling at a set velocity. However, when the UTV is driven on a slope at the set velocity, the trajectory is shifted so that the vehicle does not follow the planned trajectory. The estimated circle center coordinates for the first through third circles of travel are (8.4931, 1.4772), (8.0269, 1.6910), and (7.6030, 1.9146), respectively. The theoretical mean radii of turn for the first through third circles are 0.9482 m, 0.9480 m, and 0.9462 m, respectively. The RMSEs of the horizontal and vertical coordinates of the first trajectory are 0.9327 and 1.0483, respectively.

The experiment illustrates that an UTV traveling on a slope can experience large slips if the slope is not factored into the motion planning algorithm, causing the vehicle to travel off the desired trajectory. If the vehicle is traveling too fast, it can slip and skid, causing instability and loss of control. Therefore, it is essential to predict the amount of track sliding based on the slope-steering model when developing the UTV motion planning algorithm.

B. EXPERIMENTS TO VALIDATE THE UTV SLOPE-STEERING MODEL

The slope-steering model was embedded in the control program of the UTV. The output velocity control commands

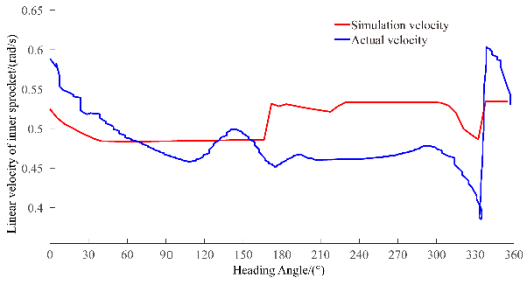

FIGURE 23. Comparison between commanded and actual inner sprocket linear velocity.

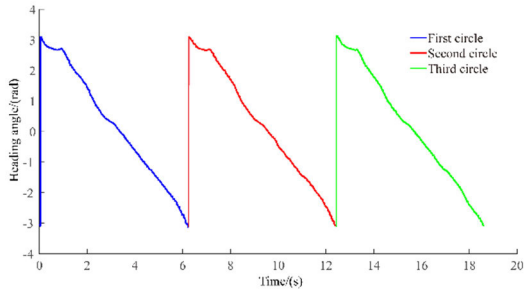

FIGURE 24. Graph of change in heading angle of UTV traveling.

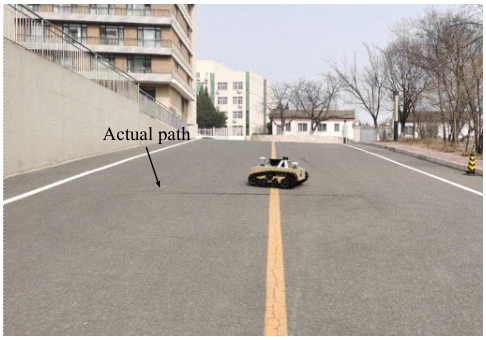

FIGURE 25. The actual path of UTV.

of both sprockets were generated in real-time to make the vehicle travel on the slope according to commands, with the predetermined velocity set to 2 km/h and a circular target path with a radii of 2 m. Figures 22 and 23 show the comparison curves between the velocity control commands generated by both sprockets according to the SSTP-RRT algorithm and the actual measured velocity values. It can be seen that the overall trend of the two curves is the same, with little difference in values, showing that the UTV can operate according to the control volume by the motion planning algorithm. Figure 24 shows a graph of the change in heading angle for three circles of vehicle travel.

Figure 25 shows a photograph of the vehicle during the experiment, where marks left by its rubber tracks can be seen on the asphalt. Figure 26 shows the actual trajectory of the UTV driving autonomously for three laps, tested by laser Lidar. The estimated circle center coordinates for the first through third driving trajectories are (7.6095, 4.9398),

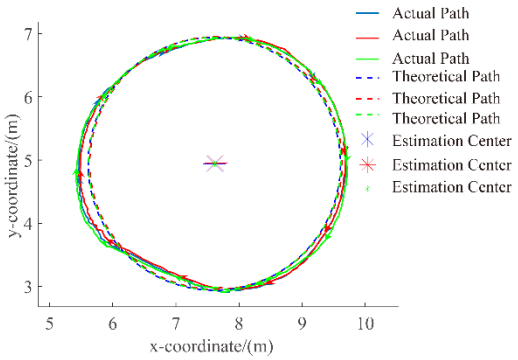

FIGURE 26. Comparison of actual and theoretical paths of UTV.

(7.6354, 4.9519), and (7.6175, 4.9414), respectively. The actual steering radii of the first circle is 2.0689 m, and the theoretical mean steering radii of the second and third circles are 2.0961 m and 2.0964 m, respectively. The RMSEs of the actual steering radii of the first through third circles are 0.1180, 0.1137, and 0.1137, respectively. The third steering radii RMSE is 0.1072.

It can be concluded that the SSTP-RRT algorithm enables an UTV to more accurately follow a planned trajectory, overcoming the effect of slope-steering track sliding on the trajectory deviation.

VI. CONCLUSION

We focused on the slope steering motion planning of UTV based on the SSTP-RRT algorithm.

We establish a high-precision UTV slope-steering dynamics model. Based on the longitudinal sliding model of UTV slope-steering, the model incorporates the factors of integrated transverse and longitudinal sliding and steering centrifugal force, and solves the initial value selection problem of the traditional nonlinear system of equations of the solution method through the PSO-LM algorithm to achieve the accurate estimation of the integrated transverse and longitudinal sliding of UTV slope-steering.

For the UTV slope-steering model, the vehicle velocity was a highly sensitive variable, and different steps were selected for pre-calculation based on the ranking of the sensitivity index, whose results were compiled into a 3D LUT, and a point cloud surface fitting algorithm based on the moving least-squares method was used to generate trajectories on both sides according to those generated by TP-RRT. Velocity planning was completed by controlling the velocities of both sprockets.

The experiment of fixing the velocity of both sprockets of an UTV showed that the tracked vehicle slipped considerably when steering on a slope, making it impossible to precisely follow the desired trajectory, and an effective and feasible solution was necessary for the motion planning of UTV slope-steering. Through the slope-steering verification experiments of the UTV, the accuracy and feasibility of the SSTP-RRT motion planning algorithm were verified, providing effective technical support for accurate UTV slope-steering. Our future

work will be to extend the algorithm to motion planning of wheeled unmanned vehicles and improve the existing algorithm using machine learning algorithms.

REFERENCES

[1] Z. Shiller, W. Serate, and M. Hua, "Trajectory planning of tracked vehicles," in *Proc. IEEE Int. Conf. Robot. Autom.*, Atlanta, GA, USA, Oct. 1993, pp. 796–801.
[2] J. Tao, H. Liu, Y. Li, H. Guan, J. Liu, and H. Chen, "Design of trajectory tracking controller of unmanned tracked vehicles based on torque control," in *Proc. IEEE Int. Conf. Unmanned Syst. (ICUS)*, Oct. 2021, pp. 85–92.
[3] Z. Ziye, L. Haiou, C. Huiyan, X. Shaohang, and L. Wenli, "Tracking control of unmanned tracked vehicle in off-road conditions with large curvature," in *Proc. IEEE Intell. Transp. Syst. Conf. (ITSC)*, Oct. 2019, pp. 3867–3873.
[4] H. Chen, "Study on path planning and location of mobile robot based on intelligent optimization algorithm," Ph.D. dissertation, College Mech. Eng., Dalian Jiaotong Univ., Dalian, China, 2018.
[5] Z. Lei, J.-Z. Fan, J. Zhao, X.-G. Wu, and Z.-F. Han, "Autonomous motion planning for obstacles-climbing of a multi-track robot," *J. Harbin Inst. Technol.*, vol. 44, no. 1, pp. 88–93, Jan. 2012.
[6] P. Peng, "The design of caterpillar track robot based on DSP," M.S. thesis, School Automat., Nanjing Inst. Technol., Nanjing, China, 2013.
[7] J. Xue-Mei, "Research on motion planning and control of mobile robot based on MT-FR," M.S. thesis, School Mech. Eng., Tianjin Univ. Technol., Tianjin, China, 2014.
[8] G. Jian, "The navigation and control technology of tele-autonomous for small tracked mobile robot," Ph.D. dissertation, School Mechatronic Eng., Beijing Inst. Technol., Beijing, China, 2015.
[9] B. Wang, H. Guan, J. Gong, H. Chen, and H. Zhao, "Unified motion planning method for heterogeneous tracked vehicles," *Acta Armamentarii*, vol. 43, no. 2, pp. 241–251, Apr. 2022.
[10] Z. Lin, "Research on path planning and trajectory tracking control method of tracked vehicles," M.S. thesis, School Mech. Aerosp. Eng. (SMAE), Jilin Univ., Changchun, China, 2020.
[11] D. Wei, "Research on path planning and trajectory tracking of tracked EOD," Ph.D. dissertation, School Control Sci. Eng., Shandong Univ., Jinan, China, 2018.
[12] S. Haohan, "Research on path planning of tracked unmanned platform in dynamic environment," M.S. thesis, Harbin Inst. Technol., Harbin, China, 2020.
[13] H. Wang, "Analyzing and testing verification the performance about high-speed tracked vehicles in steering process," *J. Mech. Eng.*, vol. 50, no. 16, p. 162, 2014.
[14] N. A. I. Ruslan, N. H. Amer, K. Hudha, Z. A. Kadir, S. A. F. M. Ishak, and S. M. F. S. Dardin, "Modelling and control strategies in path tracking control for autonomous tracked vehicles: A review of state of the art and challenges," *J. Terramechanics*, vol. 105, pp. 67–79, Feb. 2023.
[15] Y. Zhang, M. Qiu, X. Liu, J. Li, H. Song, Y. Zhai, and H. Hu, "Research on characteristics of tracked vehicle steering on slope," *Math. Problems Eng.*, vol. 2021, pp. 1–18, Jan. 2021.
[16] W. Guangfu and W. Luping, "Research on particle swarm algorithm to optimize robot path planning," *Mech. Sci. Technol. Aerosp. Eng.*, vol. 40, no. 1–7, Jan. 2021, doi: 10.13433/j.cnki.1003-8728.20200465.
[17] K. Hongwei, X. Wenping, and C. Yi, "Hybrid algorithm for aero-engine model solving based on Levenberg–Marquardt algorithm," *J. Aerosp. Power*, vol. 38, no. 2, pp. 371–381, Feb. 2023.
[18] W. Qi, "Levenberg–Marquardt method for solving nonlinear equations," M.S. thesis, School Math., China Univ. Mining Technol., Xuzhou, China, 2018.
[19] J. L. Blanco, M. Bellone, and A. Gimenez-Fernandez, "TP-space RRT—Kinematic path planning of non-holonomic any-shape vehicles," *Int. J. Adv. Robot. Syst.*, vol. 10, pp. 12–55, Jan. 2015.
[20] J.-L. Blanco, J. González, and J.-A. Fernández-Madrigal, "Extending obstacle avoidance methods through multiple parameter-space transformations," in *Proc. Intell. Robots Syst. (IROS)*, vol. 23, Jun. 2006, pp. 1–25.
[21] F. Pianosi and T. Wagener, "A simple and efficient method for global sensitivity analysis based on cumulative distribution functions," *Environ. Model. Softw.*, vol. 67, pp. 1–11, May 2015.
[22] J. L. Blanco, J. González, and J. A. Fernández-Madrigal, "Sensitivity analysis and dominant parameter estimation of wheel-terrain interaction model," *Acta Aeronautica Astronautica Sinica*, vol. 42, no. 1, pp. 1–13, 2021.
[23] J. Y. Wong and C. F. Chiang, "A general theory for skid steering of tracked vehicles on firm ground," *Proc. Inst. Mech. Eng., D, J. Automobile Eng.*, vol. 215, no. 3, pp. 343–355, Mar. 2001.

YU ZHANG received the B.S. degree in mechanical engineering from the Beijing Institute of Technology, China, in 2011, and the M.S. and Ph.D. degrees in mechanical engineering from the Army Academy of Armored Force, China, in 2013 and 2022, respectively. He is currently a Lecturer with the Department of Vehicle Engineering, Army Academy of Armored Force. His main research interests include unmanned system motion planning and environment perception.

XIXIA LIU is currently a Professor with the Department of Vehicle Engineering, Army Academy of Armored Forces, China. His main research interests include unmanned system environment perception, decision planning, and system integration.

HONGQIAN CHEN, photograph and biography not available at the time of publication.

MIANHAO QIU, photograph and biography not available at the time of publication.

YUE ZHAO, photograph and biography not available at the time of publication.

XUDONG ZHANG, photograph and biography not available at the time of publication.